Article

Not peer-reviewed version

Development and Characterization of Paclitaxel-Loaded Li-pid-Coated Mesoporous Silica Nanoparticles for pH-Responsive Tumor-Targeted Drug Delivery

Deng Yingyue , Zhou Jiaru , Zhang Tao , Wang Guoqiang , Xiao Min , Ban Junfeng , Zhang Yan * , Liang Hongcai *

Posted Date: 17 September 2024

doi: 10.20944/preprints202409.1314.v1

Keywords: Paclitaxel; mesoporous silica nanoparticles; liposomes; antitumor

Article

Development and Characterization of Paclitaxel-Loaded Lipid-Coated Mesoporous Silica Nanoparticles for pH-Responsive Tumor-Targeted Drug Delivery

Yingyue Deng [1,2], Jiaru Zhou [1,2], Tao Zhang [1,2], Guoqiang Wang [1], Min Xiao [1], Junfeng Ban [1,2], Yan Zhang [1,2,*] and Hongcai Liang [3,*]

[1] Guangdong Pharmaceutical University; Guangzhou, People's Republic of China
[2] The Innovation Team for Integrating Pharmacy with Entrepreneurship, Guangdong Pharmaceutical University, Guangzhou, People's Republic of China
[3] Guangdong Provincial Hospital of Chinese Medicine, The Second Affiliated Hospital of Guangzhou University of Chinese Medicine, Guangdong Provincial Academy of Chinese Medical Sciences, Guangzhou, Guangdong 510006, China
* Correspondence: e-mail：yanzhang@gdpu.edu.cn (Y.Z) ; lianghongcai@gzucm.edu.cn (HC.L)

Abstract: Nanoparticle carriers can selectively deliver the drug cargo to tumor cells, thus having the ability to prevent early drug release, reduce non-specific cell binding, and prolong in vivo drug retention. We constructed paclitaxel (PTX)-loaded lipid-shell mesoporous silica nanoparticles (LMSNs) for targeted anti-cancer drug delivery. The physical properties of PTX-LMSNs were analyzed by scanning electron microscopy (SEM) and transmission electron microscopy (TEM). The drug loading (DL%) and entrapment efficiency (EE%) of PTX-LMSNs were measured by high performance liquid chromatography (HPLC). In vitro drug release test, in vivo imaging, tissue distribution and pharmacokinetics of PTX-LMSNs were also evaluated. The SEM examination showed that MSNs were sphere, whereas TEM showed that they were rich in fine pores. The uniform core-shell structure of PTX-LMSNs was also verified by TEM. The DL capacity of PTX-LMSN was as high as 21.75%, and PTX was released from the nanoparticles in vitro in a pH-dependent manner. The cumulative amount of free PTX increased at lower pH, which is conducive to selective drug release from LMSNs in the acidic tumor tissues. In vivo imaging showed prolonged retention of PTX-LMSNs, which is beneficial to their therapeutic efficacy. In addition, PTX-LMSNs were primarily concentrated in the liver. Pharmacokinetic experiments showed that the half-life of PTX-LMSNs was 23.21% longer and 79.24% higher than that of Taxol. Together, LMSNs are a highly promising antineoplastic drug carrier system.

Keywords: paclitaxel; mesoporous silica nanoparticles; liposomes; antitumor; pH sensitivity; controllable drug delivery

1. Introduction

Chemotherapy is still an indispensable tool for treating advanced cancer. However, the inability of traditional anti-cancer drugs to specifically target tumor cells not only leads to serious systemic side effects but also limits their therapeutic effects. In recent years, nanoparticles-based systems, such as liposomes, polymeric micelles and polyplexes, have gained considerable interest as anti-cancer drug carriers[1-3]. Nanoscale carriers can increase the solubility of poorly soluble drugs, improve targeted drug delivery to lesions and reduce injury to normal tissues and organs. However, traditional carriers prepared by nano-preparations such as liposomes are unstable in body fluids and also release the drug cargo before reaching the tumor, resulting in serious adverse effects[4, 5]. Particle size is an important parameter for efficient delivery of nanocarriers to tumor sites, as well as for their high adsorption on the tumor cell surface, cellular uptake and intracellular transport, which eventually determine the efficacy of chemotherapy [6-8] . Nanocarriers have been designed to have

 doi:10.20944/preprints202409.1314.v

the ability to change in particle size before reaching the tumor site in response to enzyme, pH, heat and magnetism, which further affects their permeability, retention and clearance rate at the tumor site depending on the characteristics of the latter. Tong[9]. designed and synthesized hydrophobic nanocarriers that had decreasing particle size from 143.2 nm to 47.1 nm in HT-1080 tumor-bearing mice and had significantly prolonged survival time, thus could effectively inhibit tumor growth. Likewise, Nam[10] prepared and characterized gold nanocarriers with a particle size of 10 nm that expanded to 443 nm once they reached the tumor site; they had enhanced drug retention in tumor cells and could increase tumor clearance. Nevertheless, nanoparticles that are responsive to the unique characteristics of the tumor microenvironment (TME) are more effective therapeutic agents. Therefore, nanocarriers synthesized using materials that are sensitive to TME-specific stimuli and can change in particle size once they reach the tumor site. Yu[11]fabricated nanocarriers using methoxy polyethylene glycol-polylactide-polydiamino ester (MPEG-PLA-PAE) for targeted tumor delivery of a chemotherapy drug, curcumin. Loading the drug into the MPEG-PLA-PAE matrix increased its toxicity by 18% compared to that of the free drug, resulting in a tumor inhibition rate of 65.6%. The enhanced potency of the trapped drug is attributed to the decrease of the nanocarrier size from 171 nm to 22.6 nm at the tumor site, which reduces the diffusion barrier and allows the carrier to penetrate into the deep interstitial regions of the tumor, thereby effectively increasing curcumin retention. Therefore, a stimuli-responsive drug delivery system can release the drug cargo at the target site, which enhances the therapeutic efficacy and potentially reduces damage to normal tissues.

Nanocarriers have been designed to be responsive to various physical and chemical stimuli such as temperature, electric field, pH value, magnetic field and ionic strength, of which the pH value and temperature are widely applied since they do not require additional lasers and are harmless to normal tissues. Mesoporous silica is biodegradable, and the degradation product, silicic acid, can be absorbed and excreted through the urinary system. Lee [12]reported that 0.1 mg·mL−1 mesoporous silica nanoparticles (MSNs) could be completely degraded within 7 days in simulated body fluids in vitro. However, MSNs have disadvantages such as uncontrolled drug release and leakage before reaching the target. In addition, although MSNs are biocompatible, they cannot be effectively uptaken by certain types of cells[13], causing the efficacy of the drug to reduce. Nevertheless, owing to their high surface area, pore volume, uniformity, biocompatibility and biodegradability, MSNs are highly promising inorganic drug carriers[14, 15].

Lipid-shell and mesoporous silica core nanoparticles (LMSNs) combine the characteristics of nanoparticles and liposomes. The dual vesicular and particulate structure is associated with high biocompatibility, stability and favorable pharmacokinetic profile[16]. Furthermore, drugs can be efficiently encapsulated within the polymer core and/or between the lipid bilayers of LMSNs, thus allowing LMSNs to have high loading capacity. The polymer core might also delay drug diffusion and increase the stability of the lipid shell, thereby enhancing the encapsulation efficiency (EE) and system stability. While it is relatively easy to load hydrophobic drugs into LMSNs, it is challenging to achieve high EE and optimal particle size when incorporating hydrophilic drugs. To this end, our aim was to develop paclitaxel (PTX)–LMSNs with high drug EE, small particle size and enhanced tumor targeting ability. LMSNs were prepared using a modified method, and PTX-LMSNs were comprehensively characterized. The distribution of the nanovehicles in mice was observed by real time in vivo imaging. The in vivo pharmacokinetics of the drug was also evaluated.

2. Results

2.1. Characterization of MSNs and PTX-LMSNs

MSNs were morphologically characterized by SEM and TEM. As shown in the SEM images in Figure 1a, the MSNs had a uniform and regular spherical structure. Furthermore, TEM analysis verified the presence of pores on the MSNs, as indicated by the contrasting dark pore wall and bright channel in the images shown in Figure 1b. The particle diameter is about 150 nm.. In addition, the pore walls appeared distinct and were densely arranged. TEM examination of the PTX-LMSNs

 doi:10.20944/preprints202409.1314.v

(Figure 1c) revealed that they were spherical particles with a uniformly thick surface lipid layer and a distinct core-shell layer structure.

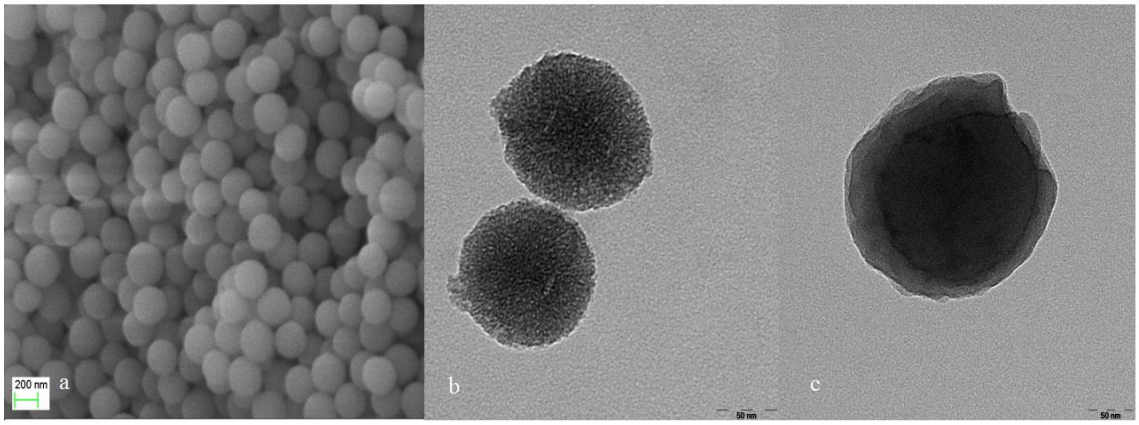

Figure 1. (a) SEM image of MSNs. (b) TEM image of PTX-MSNs. (c) TEM image of PTX-LMSNs.

As shown in Figure 2a, the average particle size of MSNs was 225.6 ± 9.44 nm, and their PDI was 0.097 ± 0.02. These numbers indicate that MSNs have high stability and uniform particle size distribution. Furthermore, MSNs had a negative charge, according to their Zeta potential (Figure 2b). PTX-LMSNs also had a uniform particle size distribution, as indicated by the single symmetrical peak (Figure 2c). The average particle size and PDI of PTX-LMSNs were 245.8 ± 3.26 nm and 0.102 ± 0.02, respectively. Although the particle size of MSNs increased as a result of lipid modification, it remained at around 220 nm. In addition, the lipid shell had no effect on PDI, indicating that the incorporation of phospholipids did not interfere with the stability of the MSNs. As shown in Figure 2d, the lipid modification also did not cause a significant change in Zeta potential, which remained in a range of -15 to -30 mV.

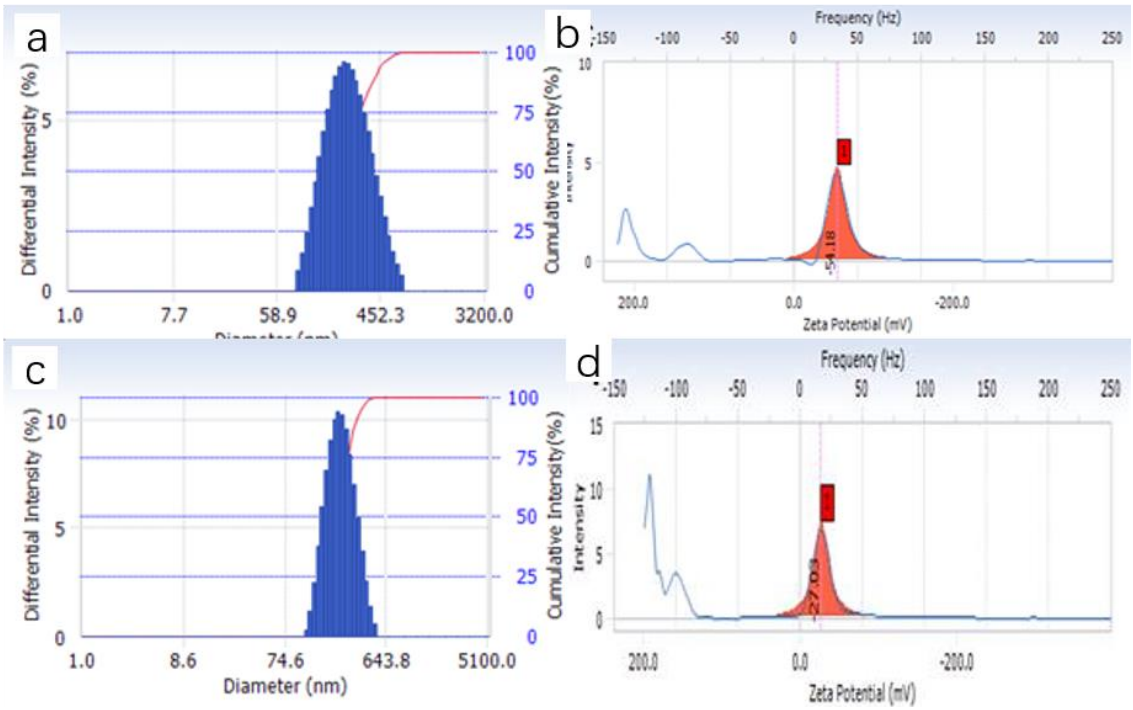

Figure 2. Particle size distribution and zeta potential of MSNs. (a) Particle size distribution of PTX-LMSNs. (b) Zeta potential of MSNs. (c) Particle size distribution of PTX-LMSNs. (d) Zeta potential of PTX-LMSNs.

 doi:10.20944/preprints202409.1314.v

According to the IUPAC nomenclature, the adsorption of MSNs belongs to a typical type IV isotherm [15] . The pore size distribution of MSN was narrow, and the average pore size was about 3.05 ± 0.04 nm, which is a suitable size allow the incorporation of PTX.

2.2. Drug Loading and Encapsulation Efficiency (EE) of PTX-LSNs

The DL and EE of PTX-LMSNs were 21.75 ± 4.28% and 96.36 ± 1.93%, respectively. This may be due to the fact that most drug molecules were loaded into the mesoporous silica pores, and only a few of them were adsorbed on the outer surface; these may cause a small amount of drug to dissociate into the solution during the preparation of lipid layer.

2.3. In vitro release of PTX from PTX-LMSNs

Unlike weakly alkaline healthy tissues, tumors have a low pH due to the Warburg effect wherein the increase of oxygen consumption leads to the production of acidic metabolites[18]. Therefore, we exposed PTX-MSNs and PTX-LMSNs to different pH levels that simulate the pH of normal tissues (pH 7.4), extracellular fluid of tumor tissues (pH 6.8) and the endosomes or lysosomes (pH 5), and then measured the amount of drug released at 37℃. As shown in Figure 3, the cumulative amount of PTX released from the LMSNs was 3-4 times higher than that released from the unmodified MSNs at all tested pH conditions, which is an indication sustained drug release. Furthermore, the cumulative amount of drug released per unit time from PTX-LMSNs was highest at pH 5: 11.48% of the encapsulated drug was released within 24 h, 22.07% within 48 h, and 43.98% within 5 d. This can be attributed to the instability of phospholipid membranes under acidic conditions [17] . Protons in an acidic medium can accelerate the replacement of the drug, thus leading to its rapid release. Therefore, the LMSN carrier is pH-sensitive and can selectively release the drug cargo at the tumor site. The cumulative increase of PTX in the acidic tumor tissues can not only improve the efficacy of the drug but also minimize the damage to normal tissues and cells.

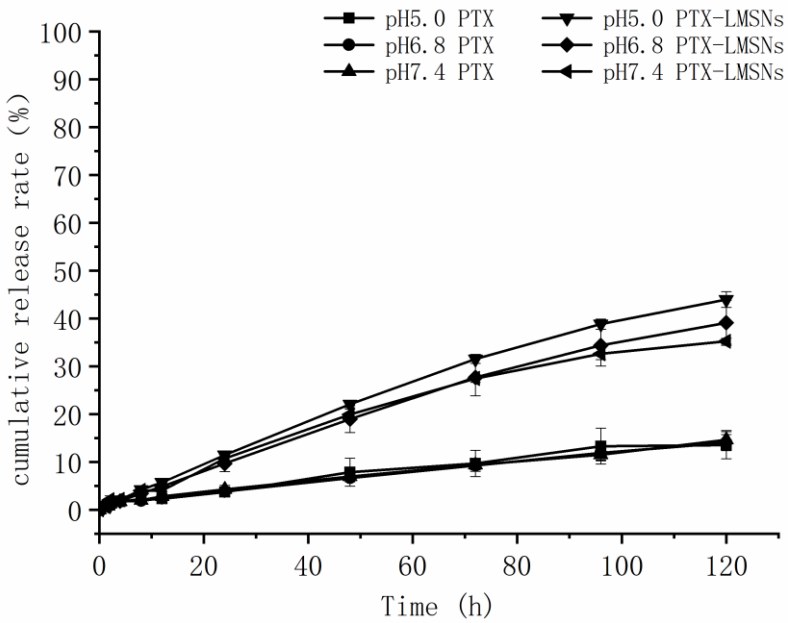

Figure 3. In vitro release profile of PTX from PTX-LMSNs under different pH conditions.

2.4. Biodistribution of Antitumor Drug in Mice

Distribution and fluorescence intensity of PTX-LMSNs in mice are illustrated in Figure 4. The probe entered the body circulation within 5 min of injection, and the fluorescence intensity of PTX-

 doi:10.20944/preprints202409.1314.v

LMSN in the abdomen increased with time and was especially high in the liver and spleen. In addition, the strong fluorescence in the bladder may be related to drug metabolism. The fluorescence intensity of PTX-LMSNs in the bladder decreased after 2 h of administration. After 6 h, fluorescence was nearly undetectable in any of the organs.

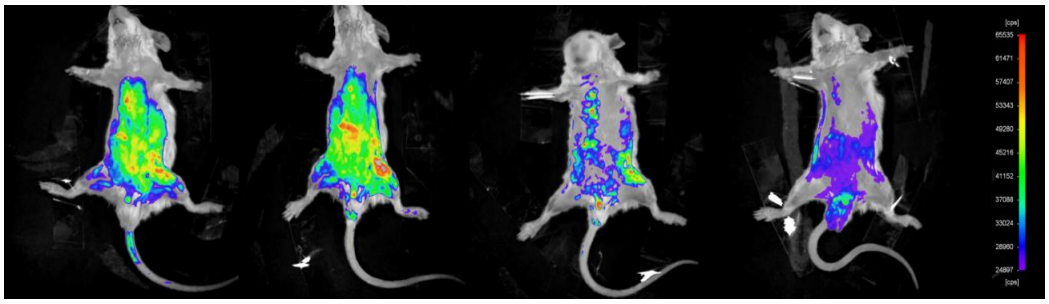

Figure 4. Distribution and fluorescence intensity of PTX-LMSNs probe in mice.

Organs were removed 6 h after administering with the PTX-LMSNs and subjected to ex vivo fluorescence imaging. As shown in Figure 5, the drug mainly accumulated in the liver, which could be due to the abundance of macrophages that can recognize opsins (serum proteins) adsorbed on the surface of the nanoparticles.

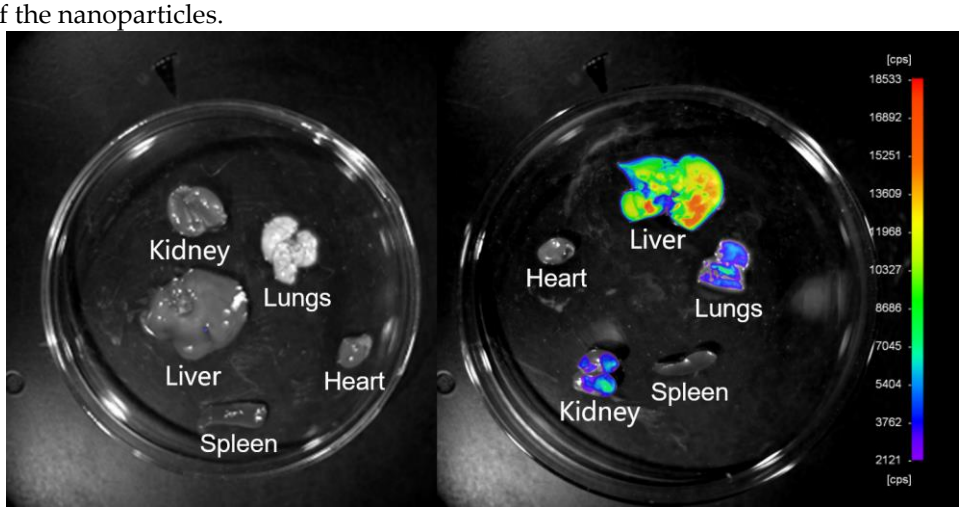

Figure 5. Tissue distribution of fluorescent PTX-LMSN (a: control; b: PTX-LMSNs).

The pharmacokinetic parameters of Taxol and the PTX-LMSNs were fitted by DAS software with the two-compartment model and are summarized in Table 1. As shown in Figure 6, the in vivo half-life of PTX-LMSNs was 23.21% higher than that of Taxol, and the area under the curve (AUC) was twice as high, an indication of longer drug retention, higher therapeutic efficacy and lower toxicity.

Table 1. Pharmacokinetic parameters in mice (n=5).

Parameters	Taxol	LMSNs
$t_{1/2\alpha}$/h	0.056	0.069
$t_{1/2\beta}$/h	1.208	0.287
Vd/L*Kg^{-1}	234.833	155.146
K_{21}/h^{-1}	4.201	5.109
K_{10}/h^{-1}	1.476	3.241
K_{12}/h^{-1}	7.363	4.157
AUC/mg·L^{-1}·h	28.848	51.707
CL/L·h^{-1}·kg	346.642	502.835

 doi:10.20944/preprints202409.1314.v

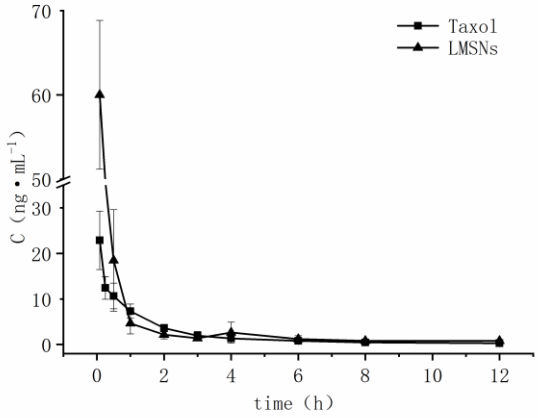

Figure 6. Concentration-time curve.

3. Materials and Methods

3.1. Materials

Paclitaxel (PTX) was purchased from Hainan Yayuan Pharmaceutical Co. Ltd. (Hainan, China), ethyl orthosilicate (TEOS) was from Aladdin Chemical Reagent Co. Ltd. (Shanghai, China), cetyltrimethyl ammonium bromide (CTAB) was from McLean Chemical Reagent Co. Ltd. (Shanghai, China), NaHCO3 was from Tianjin Zhiyuan Chemical Reagent Factory (Tianjin, China), and 15-hydroxy stearic acid polyethylene glycol (SolutolHS15) was from BASF Company. Egg yolk lecithin (PL100M) was purchased from Shanghai AVT Pharmaceutical Technology Co. Ltd. (Shanghai, China). Other chemicals and solvents were of analytical grade.

3.2. Synthesis of mesoporous silica core-lipid bilayer shell nanoparticles

The preparation of MSNs started by dissolving 1.5 g of CTAB and K2SO4 in a 255-ml solution consisting of 5 mL of 95% ethanol and 0.5 M NaHCO3 ammonia (solution 1). Solution 2 was then prepared by mixing 5 mL of 0.5 M Ca(COO)2 in 5 mL of 95% ethanol. The two solutions were quickly mixed with 10 mL of TEOS and then stirred at 600 rpm at room temperature for 6 h. After aging for 4 h, the reaction products were washed thrice with 75% ethanol at 4000 rpm, purified and then dried in vacuum at 65℃. The dried mesoporous silica carrier was soaked in 0.1 M hydrochloric acid, washed thrice with 75% ethanol at 4000 rpm, and then dried in vacuum at 65℃. Subsequently, it was calcined in a muffle furnace at 250℃ for 0.5 h and then heated to 550℃ for 4 h to obtain MSNs.

The description of lipid-modified MSNs is shown in Table 2, and the lipid-modified MSNs were prepared by post-loading method[20, 21]. Briefly, 63 mg of PTX was dissolved in 5 volumes of dichloromethane in a penicillin vial, and 3-fold MSNs were then added. The mixture was stirred at 500 rpm for 4 h in the dark at room temperature. After removing the organic solvents, 50 mL of aqueous solution containing 0.5% Solutol HS15 was poured into a round-bottomed flask, and lecithin and oleic acid were added thereafter using the membrane dispersion method. The lipids were dissolved in 25 mL of trichloromethane, and the solvent was evaporated at 40℃ until a uniform and transparent lipid film was formed. The MSN preparation was suspended in a hydration solution, and the resultant solution was poured over the lipid coating and then swirled until the lipid membrane was completely dissolved[22]. After that, it was continuously sonicated at 100 W for 5 min using an ultrasonic processor before being filtered through a 0.22 μm nylon microporous membrane. The filtrate was then added with a small volume of ampoule while passing nitrogen, and the obtained PTX-LMSNs were stored at 4℃.

 doi:10.20944/preprints202409.1314.v

Table 2. The prescription of lipid modification of mesoporous silica nanoparticles.

component	content
Paclitaxel	1.10%
MSN	3.30%
Oleic acid	0.29%
Soybean Phospholipid	2.90%
Solutol HS15	0.48%
Trichloromethane	q.s.
Dichloromethane	q.s.
water	Add up to 100%

3.3. Characterization of Nanoparticles

The morphology of MSNs was observed by scanning electron microscopy (SEM, JSM-7500F, JEOL, Japan) and transmission electron microscopy (TEM, JEM-1400, JEOL, Japan), and the morphology of PTX-LMSNs was observed by TEM. MSNs were gilded before being observed under a scanning electron microscope. The MSNs were dispersed in deionized water to a concentration of 2 mg/mL prior to TEM examination, while the PTX-LMSNs were diluted by 10 times. The particle size and polydispersion index (PDI) of PTX-LMSNs were measured by a Delsa Nano C (Beckman Coulter, USA), and their morphology was observed under a transmission electron microscope. Nitrogen adsorption-desorption was analyzed by a JWBK132F specific surface area and porosity analyzer (Beijing, China). The specific surface area was calculated by Brunauere-Emmette-Teller (BET) method, and the cumulative pore volume was calculated by Barrett-Joyner-Halenda (BJH) model.

3.4. Drug Content and Encapsulation Efficiency (EE%)

The drug loading (DL%) capacity of PTX-LMSNs was measured by high performance liquid chromatography (HPLC, 1260, Agilent Technologies, USA) using a Kromasil C18 (4.6 mm × 250 mm, 5 μm) column. The mobile phase consisted of methanol, acetonitrile and distilled water. The flow rate was 1 mL, the injection volume was 20 μL and the detection wavelength was 229 nm. To extract PTX, 1 mL of PTX-LMSN was mixed with 9 mL of acetonitrile, and the solution was filtered through a 0.22 μm membrane. The filtrate was injected into the HPLC instrument to determine the DL of PTX-LMSNs. PTX-LMSNs were extracted and separated by dextran chromatography, followed by HPLC to determine the entrapment efficiency (EE%). The SephadexG-50 separation column (1.5 cm × 13 cm) was equilibrated for 12 h before being loaded with 0.5 mL of PTX-LMSNs. The flow rate of the eluant was 3 mL/min, and the eluent was collected every 2 mL. After eluting with 30 mL of distilled water, the appropriate amount of eluent was collected and then mixed with 3 mL of acetonitrile to determine the amount of encapsulated drug (Wen). Thereafter, 30 mL of 5% sodium dodecyl sulfate (5%, v/w) was used to elute free PTX (Wfree). The EE% was calculated using the following formula:

$$EE\% = W_{en} / W_{total} \times 100\%$$

3.5. In Vitro Drug Release Assay

In vitro drug release was measured by the dialysis method. Briefly, 1 mL of PTX-LMSNs solution was loaded into a prepreg dialysis bag (molecular weight cut-off = 8000-14000). The dialysis bag was then immersed in 20 mL of buffer containing 1% sodium dodecyl sulfate with pH = 5, 6.8 or 7.4 at a constant temperature of 37℃ while gently shaken at 100 rpm. A 2-mL aliquot of sample was withdrawn at 0, 1, 2, 4, 8, 12, 24, 48, 72, 96 and 120 h and subjected to HPLC analysis. The withdrawn sample was replaced with the same volume of fresh buffer. The experiment was repeated three times. The cumulative release rate (Q) of PTX was calculated using the following formula:

 doi:10.20944/preprints202409.1314.v

$$Q = (CiV + \sum_{i=1}^{n-1} C_{i-1} \times 2)/M \times 100\%$$

where Ci is the sample concentration at the time point i, V is the volume of the suspension plus the release medium in the dialysis bag, and M is the dose of PTX in the dialysis bag.

3.6. In Vivo Biodistribution

Comply with the ARRIVE guidelines and were carried out in accordance with the U.K. Animals (Scientific Procedures) Act, 1986 and associated guidelines, and EU Directive 2010/63/EU for animal experiments. C57 Mice were depilated and anesthetized by intraperitoneal injection with 1.3 g/kg uratan solution（＞98%，65mg/mL）, and injected intravenously with 0.1 mL of fluorescent Rhodamine-LMSNs. The mice were imaged at 5, 30, 120 and 360 min post-injection and euthanized for 6 h after imaging. The heart, liver, spleen, lungs and kidneys were dissected, washed with deionized water and placed in a Petri dish. The tissues were imaged at an excitation wavelength of 550 nm and an emission wavelength of 600 nm for a fixed exposure time of 0.1 s. After the experiment, the mice were euthanized by cervical spondylolysis.

3.7. Pharmacokinetics Analysis

Animal experiments have been approved by the Institutional Animal Care and Use Committee of Guangdong Pharmaceutical University and comply with the ARRIVE guidelines and were carried out in accordance with the U.K. Animals (Scientific Procedures) Act, 1986 and associated guidelines, and EU Directive 2010/63/EU for animal experiments. SD Rats were fasted and weighed 12 h before the experiment. The animals were randomly divided into two groups (6 per group, equal number of male and female) and injected with 20 mg/kg PTX-LMSNs via the tail vein. Blood samples (250 μL) were collected via the retroorbital route at 0, 0.083, 0.5, 1, 2, 3, 4, 6, 8 and 12 h post-injection and placed in heparin-coated tubes. After the experiment, rats were euthanized by inhaling CO2.The blood samples were centrifuged at 3000 rpm for 10 min, and the upper plasma layer was collected. The plasma (100 μL) was mixed with an equal volume of acetonitrile, vortexed for 1 min, sonicated for 1 min (40 kHz, 300 W), and then centrifuged at 10000 rpm for 10 min. The samples were then analyzed by HPLC.

3.8. Statistical Analysis

SPSS17.0 statistical software was used for statistical analysis. The data were expressed as mean ± standard deviation (SD). Comparison of the tested samples with the control samples was carried out by analysis of variance and t-test. $P < 0.05$ was considered statistically significant.

4. Conclusions

We successfully prepared PTX-LMSNs by fusing liposomes with MSNs. PTX-MSNs were sensitive to low pH, making them ideal drug carriers for the acidic TME, as they could be controlled to release the drug cargo in a pH-responsive manner. The targeted delivery of the drug cargo to the tumor site improves therapeutic efficacy while minimizing damage to normal tissues. Real-time in vivo near-infrared fluorescence imaging showed a fairly board large size distribution range of PTX-LMSNs, which may be related to their low metabolism. Visceral fluorescence intensity map further indicated that PTX-LMSNs were mainly clustered in the liver. This can be attributed to the fact that the abundant macrophages in the liver can recognize opsins (serum proteins) adsorbed on the surface of the nanoparticles. In vivo pharmacokinetics showed that PTX-LMSNs had a higher AUC compared to that of Taxol, indicating that they have longer retention. This property is beneficial for high drug efficacy and low toxicity.

Funding: This work was supported by Guangdong Graduate Education Innovation Program: Project Funded by Guangdong Province Joint Training Graduate Demostration Base (Sinopharm Group Feng Liao Xing (Foshan)

 doi:10.20944/preprints202409.1314.v

Medicinal Material & Slices Co.,Ltd.)Guangdong Pharmaceutical University "Innovation and Enhancing Project".

Institutional Review Board Statement: Animal experiments have been approved by the Institutional Animal Care and Use Committee of Guangdong Pharmaceutical University and comply with the ARRIVE guidelines and were carried out in accordance with the U.K. Animals (Scientific Procedures) Act, 1986 and associated guidelines, and EU Directive 2010/63/EU for animal experiments.

Data Availability Statement: All data supporting the conclusions of this article are included within the article.

Conflicts of Interest: The authors declare that they have no competing interests.

Abbreviations

PTX	paclitaxel
MSNs	mesoporous silica nanoparticles
LMSNs	lipid-shell mesoporous silica nanoparticles
PTX-LMSNs	paclitaxel-loaded lipid-shell mesoporous silica nanoparticles
SEM	scanning electron microscopy
TEM	transmission electron microscopy
DL%	The drug loading
EE%	entrapment efficiency
HPLC	high performance liquid chromatography
TEOS	ethyl orthosilicate
CTAB	cetyltrimethyl ammonium bromide
Solutol HS15	15-hydroxy stearic acid polyethylene glycol
PDI	polydispersion index
BET	Brunauere-Emmette-Teller
BJH	Barrett-Joyner-Halenda
SD	standard deviation
AUC	area under the curve

1. References

2. Gujrati M, Vaidya A M, Mack M, et al. Targeted Dual pH-Sensitive Lipid ECO/siRNA Self-Assembly Nanoparticles Facilitate in Vivo Cytosolic sieIF4E Delivery and Overcome Paclitaxel Resistance in Breast Cancer Therapy[J]. Adv Healthc Mater, 2016,**5**(22):2882-2895.
3. Ma L, Zhang M, Yang A, et al. Sensitive fluorescence detection of heparin based on self-assembly of mesoporous silica nanoparticle-gold nanoclusters with emission enhancement characteristics[J]. Analyst, 2018,**143**(22):5388-5394.
4. Anderski J, Mahlert L, Sun J, et al. Light-responsive nanoparticles based on new polycarbonate polymers as innovative drug delivery systems for photosensitizers in PDT[J]. Int J Pharm, 2019,**557**:182-191.
5. Hobson J J, Al-Khouja A, Curley P, et al. Semi-solid prodrug nanoparticles for long-acting delivery of water-soluble antiretroviral drugs within combination HIV therapies[J]. Nat Commun, 2019,**10**(1):1413.
6. Sy P M, Anton N, Idoux-Gillet Y, et al. Pickering nano-emulsion as a nanocarrier for pH-triggered drug release[J]. Int J Pharm, 2018,**549**(1-2):299-305.
7. Mahajan U M, Teller S, Sendler M, et al. Tumour-specific delivery of siRNA-coupled superparamagnetic iron oxide nanoparticles, targeted against PLK1, stops progression of pancreatic cancer[J]. Gut, 2016,**65**(11):1838-1849.
8. Huang C, Ozdemir T, Xu L C, et al. The role of substrate topography on the cellular uptake of nanoparticles[J]. J Biomed Mater Res B Appl Biomater, 2016,**104**(3):488-495.
9. Wong A D, Ye M, Ulmschneider M B, et al. Quantitative Analysis of the Enhanced Permeation and Retention (EPR) Effect[J]. PLoS One, 2015,**10**(5):e0123461.
10. Tong R, Hemmati H D, Langer R, et al. Photoswitchable nanoparticles for triggered tissue penetration and drug delivery[J]. J Am Chem Soc, 2012,**134**(21):8848-8855.
11. Nam J, Won N, Jin H, et al. PH-Induced aggregation of gold nanoparticles for photothermal cancer therapy[J]. J Am Chem Soc, 2009,**131**(38):13639-13645.
12. Yu Y, Zhang X, Qiu L. The anti-tumor efficacy of curcumin when delivered by size/charge-changing multistage polymeric micelles based on amphiphilic poly(beta-amino ester) derivates[J]. Biomaterials, 2014,**35**(10):3467-3479.
13. Lee2009[J].
14. Kim J, Jo C, Lim W G, et al. Programmed Nanoparticle-Loaded Nanoparticles for Deep-Penetrating 3D Cancer Therapy[J]. Adv Mater, 2018:e1707557.

 doi:10.20944/preprints202409.1314.v

15. Kankala R K, Han Y H, Na J, et al. Nanoarchitectured Structure and Surface Biofunctionality of Mesoporous Silica Nanoparticles[J]. Adv Mater, 2020,**32**(23):e1907035.
16. Hoang T T, Cao V D, Nguyen T, et al. Functionalized mesoporous silica nanoparticles and biomedical applications[J]. Mater Sci Eng C Mater Biol Appl, 2019,**99**:631-656.
17. Kim S, Diab R, Joubert O, et al. Core-shell microcapsules of solid lipid nanoparticles and mesoporous silica for enhanced oral delivery of curcumin[J]. Colloids Surf B Biointerfaces, 2016,**140**:161-168.
18. Esparza JM, Ojeda ML, Campero A, et al. Development and sorption characterization of some model mesoporous and microporous silica adsorbents. Proceedings of the Third San Luis Symposium on Surfaces, Interfaces and CatalysisJournal of Molecular Catalysis A: Chemical. 2005. 228(1): 97.
19. Rizzo R, Onesto V, Forciniti S, et al. A pH-sensor scaffold for mapping spatiotemporal gradients in three-dimensional in vitro tumour models[J]. Biosens Bioelectron, 2022,**212**:114401.
20. Moholkar D N, Sadalage P S, Havaldar D V, et al. Engineering the liposomal formulations from natural peanut phospholipids for pH and temperature sensitive release of folic acid, levodopa and camptothecin[J]. Mater Sci Eng C Mater Biol Appl, 2021,**123**:111979.
21. Huang R, Shen Y W, Guan Y Y, et al. Mesoporous silica nanoparticles: facile surface functionalization and versatile biomedical applications in oncology[J]. Acta Biomater, 2020,**116**:1-15.
22. Laranjeira M S, Ribeiro T P, Magalhaes A I, et al. Magnetic mesoporous silica nanoparticles as a theranostic approach for breast cancer: Loading and release of the poorly soluble drug exemestane[J]. Int J Pharm, 2022,**619**:121711.
23. Lin J, Cai Q, Tang Y, et al. PEGylated Lipid bilayer coated mesoporous silica nanoparticles for co-delivery of paclitaxel and curcumin: Design, characterization and its cytotoxic effect[J]. Int J Pharm, 2018,**536**(1):272-282.